Chapter

Rational Design and Advance Applications of Transition Metal Oxides

Muhammad Ikram, Ali Raza, Jahan Zeb Hassan, Arslan Ahmed Rafi, Asma Rafiq, Shehnila Altaf and Atif Ashfaq

Abstract

An attractive class of transition metal oxides (TMOs) have been freshly concerned with increasing research interest worldwide concerning stoichiometric and non-stoichiometric configurations as well, that usually exhibits a spinel structure. These TMOs will contribute substantial roles in the production of eco-friendly and low-cost energy conversion (storage) devices owing to their outstanding electrochemical properties. The current chapter involves the summary of the latest research and fundamental advances in the effectual synthesis and rational design of TMOs nanostructures with meticulous size, composition, shape, and micro as well as nanostructures. Also applications of TMOs such as effective photocatalyst, gas sensing, biomedical, and as an electrode material that can be utilized for lithium-ion batteries, and photovoltaic applications. Additionally, certain future tendencies and visions for the development of next-generation advanced TMOs for electrochemical energy storage methods are also displayed.

Keywords: transition–metal oxides nanostructures, oxides structures, lithium-ion batteries, gas–sensing, photovoltaics

1. Introduction

One of the motivating classes of material comprises transition metal oxides (TMO) that display an assortment of properties and structure as well (0–3). The nature of bonding present among metal and oxygen can be fluctuating from partially ionic to extremely covalent (or metallic). Owing to possess outer d-electron nature the properties of TMO are unusual. The remarkable wonder of TMO is its phenomenal array of electronic as well as magnetic properties. Therefore, oxides exhibiting metallic behavior such as RuO_2, $LaNiO_3$, and ReO_3 are found at one class while oxides displaying extremely insulating properties including $BaTiO_3$ are recognized as the other one [1, 2]. TMOs can be documented as the class of oxides that comprises of cation which has incompletely or partially filled d shell. This nature is due to their marvelous feature as they are motivating and scientifically supreme category of versatile solids. This class contains a wide-range of color, magnetic, and electric properties along with most researched classes to progress their

understanding of nature. As mentioned, their bonding fluctuates from partially ionic as in case of NiO and CoO to highly covalent such as OsO_4, and RuO_4.

Furthermore, metallic bonding also arises such as TiO, ReO_3, and NbO. The crystal structure of TMOs varies from cubic symmetry to triclinic [3–5]. Further, binary oxides with the composition pattern of MO are commonly found to attain rock salt structure; but MO_2 type composition involves rutile, fluorite, distorted rutile (complex structure). Possibly, significant features of TMOs are their aptitude to bear huge withdrawal from stoichiometry that is result of cations with variable valency. As an example, a portion of cuprous ion in copper (I) oxide (Cu_2O) can be oxidized to cupric form that resulted in $Cu_{2-x}O$ which is a metal deficient composition. Similarly, ferric ion in iron (III) oxide (Fe_2O_3) can be reduced to resulted ferrous form, resulted in $Fe_{2+x}O_3$ which are metal-rich composition [6–8]. Withdraw from stoichiometry in the case of non-TMOs that includes MgO is usually appeared as small and in the order of 10^{-4}% even at an extreme temperature usually greater than 1700 °C. Other than this, TiO_2 can put up roughly 1% of oxygen vacancies as well as titanium interstitials. There are exemptions to precede this generalization, as an example, ZnO which does not correspond to the tree of TMOs can provide a departure from the stoichiometric composition that varies from the range 10^{-2} to 10^{-1} at the temperature of 1000 °C [9–11].

This exhibition from ZnO is due to its wurtzite crystal structure that involves unoccupied interstices in the lattice of oxygen which is accomplished of acquiescent interstitial zinc. This phenomenon exhibits the importance of variable valency and crystal structure for the determination of specific oxide to bear substantial non-stoichiometry. This involves the zone of defect chemistry that solid-state chemist has focused devotion to the TMOs, in certain with the impartial of classifying the kinds of defect that are existing and their equilibrium concentrations as well. At the low concentrations conditions such as ~10^{-4}% and point defects that comprise vacant sites (interstitial ions or atoms) are effectively treated via statistical thermodynamics [8, 11]. Furthermore, at the higher concentrations conditions such as ~10^{-2}%; where certain association arises, the same method can be allowed to legal. This is due to the ionic defects that origins disturbances to the crystal's electronic structure. Moreover, an influential instrument in the study of defect chemistry contains the measurement of variations in semi-conductivity that is subsequent from fluctuations in defect concentration. These variations are followed as a function of temperature, and equilibrium oxygen partial pressure [8, 12].

Statistical thermodynamic handling of the defect equilibrium is typically unsuitable at the range of high defect concentrations that turn into the development of an identifiable superlattice. Owing to these conditions, the area of oxide covering the superlattice can be viewed as a different segment and the whole non-stoichiometry of oxide can be viewed as ascending from the mixture of such segments (two or more), instead of the arbitrary circulation of defects through single segment [8, 9]. These sorts of super-lattice assembling are thought to occur in high-temperature segment CeO_{2-x}; this involves the dissociation upon chilling into a two-phase mixture that comprises CeO_2 and $Ce_{32}O_{58}$. Meanwhile, in 1950, the idea about the crystallographic shear has been familiarized as well as recognized to designate the great withdrawals from stoichiometry detected in certain TMOs. Magnéli pronounced the nature of non-stoichiometry in the MoO_3 employing these shear structures [12–14].

2. Structure determination techniques

The bulk MO structures have been regulated with broad and extremely precise XRD crystallographic plane studies [15]. Unluckily, inorganic structural chemistry

related to MO dehydrated surface around oxide sustenance cannot be evaluated with XRD owing to the nonexistence of extensive range order which is greater than 4 nm in the surface MO over the layers. Native structures of MO dehydrated surface possibly bring into being via *in situ* molecular approaches of MO dehydrated supported with respect to spectroscopic analysis: Raman [16], UV–vis, infrared, chemi-luminescence, NMR established with solid-state assembly and XANES or EXAFS, for certain nuclei including ^{51}V, ^{95}Mo, ^{1}H, etc. These characterizations approachs offer structural particulars about numeral of O atoms coordinated to a cation for example MO_4, MO_5, MO_6, and finally, M–O–M like symmetry that represent the incidence of adjacent neighbors. These kind of bridging among M–O–M bonds linkage are effortlessly obvious with Raman analysis; furthermore, this is likewise infrequently obvious for the overtone section of IR. Coupled Raman, the IR fingerprints, as well as isotopic oxygen exchange readings, are capable to begin the numeral of M = O which is pronounced as terminal bonds as an example for mono-oxo its linkage is M = O, dioxo bridging is related to O = M = O and finally tri-oxo $M(=O)_3$ [17]. The isolated mono-oxo structures consist M = O symmetric stretch v_s and it seems at a similar frequency for both approaches including Raman and IR analysis. Additionally, overtone section of IR reveals simply one band around $2v_s$. Subsequently, isolated di-oxo structures consist of the O = M = O functionality owns both stretching modes firstly, v_s termed as symmetric and secondly, v_{as} pronounced as asymmetric mode that can be disconnected through 10 cm^{-1}. IR overtone region displays three bands around $\sim 2v_s$, $v_s + v_{as}$, and $\sim 2v_{as}$ with extent upto ~20 cm − 1 assortments. For isolated tri-oxo functionalities, more complex vibrational spectra appear and several bands will usually present in overtone, and stretching regions. Raman is normally quite sensitive to v_s whereas IR is sensitive to v_{as}. The moment when O = M = O bonds are detached through 90°, then splitting of bands will not be perceived and the vibrations will degenerate [18]. Isotopic ^{16}O or ^{18}O exchange readings are capable to divide such kinds of degenerate vibrations through isotopic scrambling for oxygen. Mono-oxo structures correspond to two kinds of bands that are associated with symmetrical stretching mode and it will be existing owing to the vibration of M = ^{16}O, and M = ^{18}O as well. For di-oxo structures, three kinds of bands (symmetric stretching) will perform owing to firstly, ^{16}O = M = ^{16}O secondly, ^{18}O = M = ^{18}O, and thirdly, ^{16}O = M = ^{18}O vibrations. Besides, these fourth bands (symmetric stretching) should seem for tri-oxo functionalities which contains the vibrations of firstly $M^{16}O_3$, secondly, $M^{18}O^{16}O_2$, thirdly, $M^{18}O^{16}{}_2O$, and lastly $M^{18}O_3$). Additionally, isotopic swings owing to the replacement of the heavier ^{18}O with the ^{16}O isotope can correspondingly evaluated for oscillators based upon diatomic materials and it also matched with the detected isotopic shifts. Therefore, grouping of such sorts of measurements taken from the analysis of molecular spectroscopy which is combined with isotopic O atom exchange readings stay mandatory to achieve structures that are absolutely linked with MO dehydrated surface [3, 15, 19].

2.1 V^{5+} oxides

Inorganic chemistry of bulk vanadium with respect to its structural analysis that possesses the oxidation state of +5 is the greatest diverse between bulk MO. Additionally, this analysis has been evaluated from the broad-ranging examination of XRD. Further, Bulk vanadate (VO_6) ions comprise of firstly, isolated orthovanadate (VO_4^{3-}) secondly, dimeric pyrovanadate ($V_2O_7^{4-}$), or polymeric chain which is metavanadate $(VO_3)_n^{n-}$ structures. These four-coordinated vanadate ions are distinguished through amount of linking bonds with an assembly of V–O–V are existing firstly, orthovanadate (0) secondly, pyrovanadate (1), and finally metavanadate (2) structures. The charge in their structures is balanced via

cations (e.g., Na_3VO_4, and $Na_4V_2O_7$,). Bulk vanadate's (VO_6) exhibits quite collective structures, which are normally, bring into extended structures of vanadia. As an example, decavandate cluster present in $Na_6V_{10}O_{28}$ contains five discrete distorted sites of VO_6 [20]. The extremely distorted VO_6 structures typically retain one V=O (terminal bond) of the type mono-oxo) having bond lengths ranges from 0.158 to 0.162 nm. In certain greatly distorted oxides of VO_6, the sixth oxygen is positioned far away from vanadium atom in such a way that these compounds are efficiently reflected to hold VO_5 coordination. Numerous gas-phase $X_3V=O$ mono-oxo halide classes are also recognized and vanadyl vibrations ranges in the order of 1025–1058 cm^{-1} that owns growing electronegativity of respective halides species which follows the sequence Br < Cl < F [21]. The oxyhalide vibrations of $F_2V\,O_2^-$ and $Cl_2V\,O_2^-$ that belongs to di-oxo are detected at two reading firstly, at 970/962 and secondly at 970/959 cm^{-1}. As a conclusion, bulk vanadium that owns +5 oxidation state and holds rich inorganic chemistry is assembled up from the coordinated structures of VO_4, VO_5, and VO_6 (see **Figure 1**).

2.2 Cr^{+6} oxides

Bulk chromates hold CrO_4 coordination in isolated mono-chromate (CrO_4), dichromate (Cr_2O_7) that termed as dimer, tri-chromate (Cr_3O_{10}) which is designated as trimer, and tetr-achromate (Cr_4O_{13}) which is named as tetramer with infinite chain CrO_3 (polychromate or metachromate) structures [22]. In contrast to the respective bulk vanadates, bulk non-CrO_4 comprising structures are unidentified as an example CrO_5 and CrO_6 (see **Figure 2**). The crystalline structure of CrO_3 is assembled up of countless chains via connecting CrO_4 entities comprised of two short bonds (0.160 nm) and two extended bonds (0.175 nm). These entities are lonely apprehended with each other via van der Waal interactions. Infrequent short MP of CrO_3 is 197 °C reveals weak van der Waal forces between poly-chromate chains. Bulk CrO_3 attaining faint thermal stability is also reflected in its superficial lessening and the decomposition to respective bulk Cr_2O_3, which contains only Cr with +3 oxidation state as cations. The Cr with an oxidation state of +6 is generally unchanging through the existence of non-reducible cations that include As, K, P, Rb, and Na. Chromium oxy-halides that correspond to gas-phase are also recognized and vibration of mono-oxo $F_4Cr = O$ are detected around 1028 cm^{-1}, while the vibrations associated with di-oxo $F_2Cr(=O)_2$ are identified around 1006 cm^{-1} for υ_s as well as 1016 cm^{-1} for υ_{as}. Additionally, vibrations of di-oxo $Cl_2Cr(=O)_2$ are noticed around 984 cm^{-1} for υ_s as well as 994 cm^{-1} for υ_{as}. Lastly, vibrations of tri-oxo $CsBrCr(=O)_3$ around 908 for υ_s, 933, 947, and 955 cm^{-1} for υ_{as} [23]. These vibrational frequency swings as a function of the M = O bonds are pointedly away from the expected value that was imagined for dissimilar halide ligands as the gas-phase vanadyl oxy-halide complexes swing downward to 23 cm^{-1} by reflecting the shift from F-Cl ligands and downward to 10 cm^{-1} by considering the shift from Cl-Br ligands. Thus, aggregation of the amount of chromyl bonds swings leads to the corresponding vibrations to inferior wavenumbers and gradually upturns the

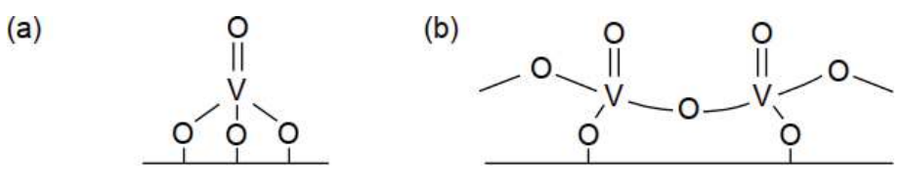

Figure 1.
Structures of (a) dehydrated isolated and (b) polymeric surface monoxo VO_4 species [15].

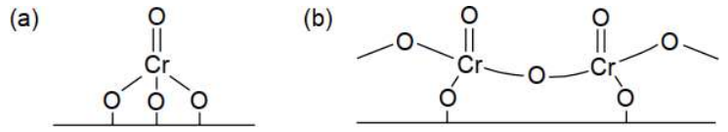

Figure 2.
Structures of (a) dehydrated isolated and (b) polymeric surface monoxo CrO_4 species [15].

sum of vibrational bands. In summary, inorganic chemistry of Cr with respect to structural analysis that owns an oxidation state of +6 chromates essentially consists of CrO_4 units with different extents of polymerization [24, 25].

Spectroscopic measurements of the dehydrated supported chromates with EXAFS or XANES, UV–vis, and chemiluminescence, exposed that dehydrated surface chromates hold CrO_4 coordination and are stabilized as Cr(+6) at prominent temperatures through oxide supports under monolayer surface exposure. Above the monolayer surface coverage, the excess chromium oxide that resides on the surface chromium monolayer becomes reduced at elevated temperatures in the oxidizing environments and forms Cr(+3) Cr_2O_3 crystallites. Thus, the surface species of Cr with oxidation of +6 are lonely steady around elevated temperatures by coordination to the oxide substrates. For non-SiO_2 supports, the Raman measurements and the IR fingerprints reveal two resilient bands around 1005–1010 cm^{-1}, as well as 1020–1030 cm − 1 and the corresponding overtone, ranges for these two bands in vibrational regions of 1986–1995 plus 2010–2015 cm^{-1}. The vibrational alteration is reliable with di-oxo functionality however; it lies faintly on the higher side [26, 27].

2.3 Re^{+7} oxides

The bulk rhenium regarding its inorganic chemistry that possesses +7 oxidation states is slightly sparse. Numerous ortho-rhenate compounds covering isolated units of ReO_4 which are somewhat common: $KReO_4$, $NaReO_4$, and NH_4ReO_4. Bulk Re_2O_7 holds a layered structure comprising of interchanging groups of ReO_4 and ReO_6, along with subunits of rings that are constituted two groups of both ReO_4 and ReO_6. The weak bonding among rhenium oxide groups in the layered structure of Re_2O_7 consequences in the effective vaporization of Re_2O_7 dimers that hold two groups of ReO_4 bridged through one O atom for example gaseous $O_3Re–O–ReO_3$. The supreme possible surface ReO_x attention on oxide supports is permanently reduced than monolayer attention due to the surface ReO_x species association to produce volatile dimers (Re_2O_7) at extreme surface coverage. Moreover, crystalline Re_2O_7 is not ever perceived as this MO is not stable to higher calcination values along with the introduction to ambient moisture. Therefore, mono-layer ReO_x with its surface coverage is not ever gotten because crystalline Re_2O_7 and volatilization does certainly not exist. Hence, supported ReO_x catalysts are exceptional between the sustained MO catalysts. In this materialization, only surface ReO_x attention below single-layer can be accomplished deprived of the occurrence of crystallites [15, 28, 29].

2.4 Mo^{+6} oxides

Bulk polymolybdate chains typically comprise MoO_6 coordinated units that are different from the chains of polyvanadate as well as polychromate and these chains are respectively possessed with VO_4 and CrO_4 groups. This reveals the liking of molybdates for greater coordination groups in comparison with vanadates and chromates units in the respective polymeric structures. Yet, certain exemptions occur to this tendency in the structural chemistry of bulk molybdate. Short coordinated molybdates exist in the dimer of MoO_4 which is $MgMo_2O_7$ and in the chain of

interchanging MoO_4 and MoO_6 units which are $NaMo_2O_7$. Coordination of isolated MoO_4 is still somewhat mutual for ortho-molybdates as an example $MgMoO_4$, $CuMoO_4$, Na_2MoO_4, $MnMoO_4$, K_2MoO_4, and $CaMoO_4$. Extremely misleading coordination of isolated MoO_4 is discovered in $Gd_2(MoO_4)_3$, $Fe_2(MoO_4)_3$, $Cr_2(MoO_4)_3$, and $Al_2(MoO_4)_3$. Whereas, extremely misleading units of MoO_5 are existing in $Bi_2(MoO_4)_3$ [20, 30]. Further, clusters of polymolybdate are constituted with 6 to 8 MoO_6; whereas coordinated units are also recognized for example $(NH_4)_4Mo_8O_{26}$, $(NH_4)_6Mo_7O_{24}$, and $[NH_3P_3(NMe_2)_6]_2Mo_6O_{19}$. Bulk MoO_3 (alpha) is comprised of a 3D structure prepared up of extremely misleading units of MoO_6. The great misleading existing in bulk MoO_3 (alpha) origins the sixth O atom to be positioned extremely distant respected to Mo and, therefore, the structure of the relevant bulk MoO_3 (alpha) is well pronounced as comprising of MoO_5 units. The bulk MoO_3 (beta) crystalline period is one more MoO_3 3D structure fabricated up of minute misleading of MoO_6 units [31]. Numerous gas-phase mon-oxo molybdenum oxyhalides ($X_4Mo = O$) are also recognized, structural analysis illustrated in **Figure 3**. The Mo = O vibrations fluctuate in the range 1008–1039 cm^{-1} with the increment in electronegativity of halide in the order Cl < F. The gas-phase di-oxo $Br_2Mo(=O)_2$ growths to the bands at 995 (v_s) as well as 970 (v_{as}) cm^{-1} owing to an order of electronegativity as Br < Cl < F. Therefore, the structure of molybdenum oxides with respect to its inorganic chemistry involves the coordinated units as MoO_4, MoO_5, and MoO_6, with a first choice in polymolybdates for MoO_6 latter [32].

For non-SiO_2 supported MoO_x catalysts, MoO_x coordination for the dehydrated surface is subjected to the exposure of surface molybdena and particular oxide support. At faint surface coverage of molybdena that ranges from 5–15% of a monolayer, mainly surface coordinated groups of MoO_4 are exist on Al_2O_3 and TiO_2. The parallel Raman spectrum of the above-discussed catalysts also agrees to the extent of minute surface coverage. In addition, MoO_4 surface species are correspondingly isolated on both oxide supports. This phenomenon is also authenticated through UV–vis spectra that display huge bandgap energy related to isolated classes. Species with monolayer owns the surface exposure of molybdena, sustained MoO_3/TiO_2 was establishing to hold MoO_6 coordinated groups, and sustained MoO_3/Al_2O_3 was set up to retain a combination of MoO_4 as well as MoO_6 coordinated species. For monolayer MoO_3/Al_2O_3, the supplementary occurrence of surface MoO_6 was also revealed in minor bandgap value of this catalyst. Therefore, UV–vis analysis and Raman measurements for samples discussed above (dehydrated MoO_3/ZrO_2 and MoO/Al_2O_3) were quite alike and recommend the similar surface species such as MoO_x occur on the supports together by a certain surface exposure. Measurements are taken from Raman approach also discloses characteristics of linking Mo–O–Mo bonds existing in polymolybdates [33–35].

2.5 W^{+6} oxides

The structure of tungsten oxide concerning its inorganic chemistry carefully reflects molybdenum oxide. Numerous ortho-tungstate compounds such as Cs_2WO_4, Li_2WO_4, Rb_2WO_4, Na_2WO_4, and Na_2WO_4 holds isolated sites for WO_4

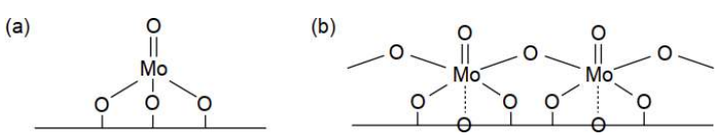

Figure 3.
Structures of dehydrated surface monoxo MoO_x species (a) isolated monoxo MoO_4/MoO_5 and (b) polymeric monoxo MoO_6 [15].

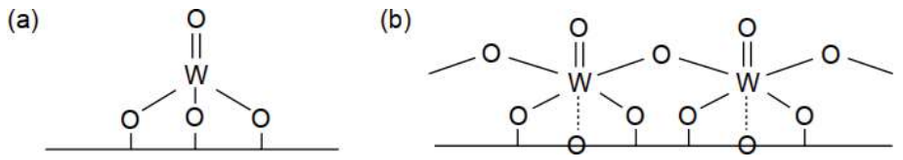

Figure 4.
Structures of dehydrated surface monoxo WO_x species. (a) Isolated surface monoxo (WO_4 and WO_5) and (b) polymeric surface monoxo surface [15].

that are identified. Infrequently tungstate compounds procedure polymeric WO_4 compounds as illustrated in **Figure 4**. One exception related to it is MgW_2O_7 that involves couples of distributing WO_4 units. Interchanging polymeric sites of WO_4 and WO_6 are existing in the poly-tungstate chains of $Na_2W_2O_7$ as well as $(NH_4)_2W_2O_7$. $Ca_3(WO_5)Cl_2$ is the compound in which presence of an isolated WO_5 coordinated site has been governing. Coordinated units of Isolated WO_6 are found in the Wolframite structure such as $ZnWO_4$, $FeWO_4$, $NiWO_4$, $MnWO_4$, and $CoWO_4$. Poly-tungstate chains are consistent with coordinated units of WO_6 which are existing in $Li_2W_2O_7$ and $Ag_2W_2O_7$. Clusters of Tungsten oxide comprises polymeric units of WO_6 which have been recognized with fluctuating the number of tungstate units: 12-membered includes para-tungstate $(NH_4)_{10}(H_2W_{12}O_{42}.10H_2O$ and meta-tungstate $(NH_4)_6(H_2W_{12}O_{40})$, 10-membered involves $NH_4BuW_{10}O_{32}$, 6-membered comprises $(NBu_4)_2W_6O_{19}$, and 4-membered consist of $Ag_8W_4O_{16}$. Furthermore, bulk WO_3 is assembled up of 3D structure of somewhat misleading WO_6 units. Numerous gas-phase mono-oxo tungsten oxyhalides ($X_4W{=}O$) are identified such as X = F, Cl, and Br [36, 37]. The gas-phase complex of $F_4W{=}O$ displays its W=O vibrations at 1055 cm^{-1} unfortunately the vibrations of the gas phase monoxo complexes $Cl_4W{=}O$ and $Br_4W{=}O$ have not been experimentally determined. However, it is probable to approximate the vibrational frequency through the likeness with the corresponding oxy-halides such as X_4Mo = O and $X_3V{=}O$ that are correspondingly guided via electronegativity order of the halide ligands. This kind of assessment proposes the mono-oxo W=O vibrations for oxy-halides such as $Cl_4W{=}O$ and $Br_4W{=}O$ must arise respectively around 1024 and 1010 cm^{-1}. Furthermore, vibrational spectra analysis of $X_2W(=O)_2$ oxy-halides (di-oxo) have not been regulated, but IR fingerprints for $Br_2Mo(=O)_2$ have been reported and display their v_s/v_{as} vibrations in the range 995/970 cm^{-1}. Same values for the ions such as $[Se_2Mo\ (=O)_2]^{2-}$ and $[Se_2W(=O)_2]^{2-}$ are respectively observed around 864/834, and 888/845 cm^{-1} [38, 39]. It is worth mentioning, that the selenium covering di-oxo ions display alike vibrations. Beyond this range of W-containing ion vibrates lies in the order 10–24 cm^{-1} which is greater related to agreeing to Mo-containing ion. From this discussion, it can be suggested that oxy-halide of gas-phase $Br_2W(=O)_2$ would vibrate in the range 1020/980 cm^{-1} by similarity with $Br_2Mo(=O)_2$ [40, 41].

3. Synthetic approaches

To prepare transition metal oxides, a variety of routes can be employed such as high temperatures and pressures, hydrothermal conditions, controlled reducing and oxidizing atmospheres, and so on. A ceramic method is commonly utilized to prepare these oxides, involving continuous grinding and heat treatment of reactant materials (e.g. carbonates, oxides, etc). These oxides have got the attention to prepare under the suitable conditions of milder and minor energy-consumption. For homogeneous mixing of reactants on an atomic scale, precursor method has been utilized [42]. Compared to ceramic technique, diffusion distance is effectively diminishes by this approach from 10,000 Å to 100 Å. Furthermore, solid solutions

of hydroxides nitrates, and carbonates, have been frequently utilized to aim for this purpose besides the precursor compounds. Novel oxides that acquire challenging scheme to prepare can also be synthesized by this method. Similarly, topochemical reactions produce rare oxides such as synthesis of MoO_3 and ReO_3 structure by topochemical dehydration. By this dehydration reaction, $Mo_{1-x}W_xO_3$ has also been synthesized. Further examples of synthesizes of rare oxides by topochemical reaction are reported in the literature [43]. A worth mentioning topochemical reaction is the addition of atomic species in oxides hosts. Thus, alkali metals and lithium have been injected into the different types of oxides such as MnO_2, Fe_3O_4, TiO_2, VO_2, and ReO_3. In the literature, intercalation phenomenon has been reviewed sufficiently. By employing slight oxidizing conditions, deintercalation of lithium and some alkali metals can be carried out steadily. Several innovative examples of deintercalation and intercalations phenomenons are being continuously conveyed. Recently, lithium injection to $W_{19}O_{55}$ and topochemical reactions of Li_xNbO_2 has been reported. Ion exchange can be executed in the close-packed arranges of oxides, tunnel and layered structures. These reactions are also associated as topochemical and can be executed in molten media e.g., conversion to $HNbO_3$ from $LiNbO_3$ with hot aqueous acid [44]. The procedure of this reaction is contrary to transformation of ReO_3 to $LiReO_3$ (rhombohedral). Hydrogen can also be injected into holes of oxide with the company of Pt catalyst. Diversities of exchange reactions are huge for synthetic purposes. In the literature, many exchange reactions have been mentioned; two recent examples are given as the exchange properties of $Na_4Ti_9O_{20}$ (X) H_2O and intercalated effect of alkylammonium ion on cation (+) exchange properties of $H_2Ti_3O_7$. Preparation of layered $K_2Ti_4O_9$ and metastable TiO_2 using a topotactic dihydroxylation is also an interesting example [42, 45].

The vapor deposition method is a well-known technique among other synthesis methods. Complex oxides (Mo and Mo bronzes) have been synthesized by employing fused salt electrolysis. Under oxidizing conditions, the pyrochlores $Bi[Ru_{2-x}\,Bi_x^{5+}]O_{7-Y}$ and $Pb_2[Ru_{2-x}\,pb_x^{4+}]O_{7-Y}$ has been synthesized from an alkaline medium [45, 46]. The sol–gel approach is more efficient in preparing multiple oxides and superconducting cuprates. Although arc melting process can prepare many oxides a novel technique is a crucible-free method. Synthesis by high-pressure methods has been reviewed. This greater pressure reasons to stabilize the states of rare oxidation (e.g. $GdNiO_3$, $La_2Pd_2O_7$, etc.). Recently, under high oxygen pressure $YBa_2CU_4O_8$ has been synthesized [45, 47, 48].

3.1 Transition–metal oxides nanostructures

Ended to the previous few decades, transition metal oxides nanostructures (TMON) have been extensively considered owing to attain excessive potential in optical, electronic, and magnetic applications. To accomplish extraordinary and exceptional performances, TMONs have been assimilated into the assortment of devices that consists of efficient photocatalysis, and enhanced gas sensing [49, 50]. In TMOs, although the electrons are permanently occupied in the s – shells of +ve metallic ions, the d – shells of TMOs may not be entirely occupied. This distinctive carries numerous exceptional properties in them, that comprises decent electrical characteristics [51–53] high dielectric constants [54, 55], reactive electronic transitions [56, 57], wide band gaps [58, 59], and so on. Meanwhile, TMOs owns several states including, ferrimagnetic, ferromagnetic, and semi-conductive state. Hence, TMOs are reflected in the absolute interesting functional materials. Catalysts are liquefied into liquid alloy droplets, which also comprise corresponding source metal. When alloy droplets attain supersaturated condition then the respective source metal initiates to precipitate which turns into metal oxide followed by the flow of

oxygen. Generally, as–synthesized metal oxides especially rise along specific alignment, which resulted in the establishment of 1D nanostructure. Up to now, preparation approach for the metal oxide nanowires including In_2O_3, [60] CdO [61], TiO_2 [62], ZnO [63], and SnO_2 [64] have been accomplished using VLS mechanism. The VLS procedure corresponds to catalyst–aided growth whereas; VS route is attributed to the catalyst–free growth [65, 66]. The progression of VS method includes the reactants which are first heated to produce vapors followed by high temperature and then unswervingly condensed on the substrate. In this substrate, the seed crystals will be assisted to nucleation sites located and acquire shape. Facilitate directional growth followed will minimize the surface energy of product.

In 1970s, the hydrothermal route was primarily hired to synthesize the various types of crystalline structures. Using this strategy, reactants are positioned in the sealed vessel that followed water as the solvent (reaction medium). A reaction in hydrothermal approach proceeds in the presence of high temperature that causes to produce high pressure. This procedure can speed up the reactions among ions and finally endorse the hydrolysis. Eventually, self–assembly, as well as the growth and of crystals, will be succeeded as the consequence of reaction mechanism in solution. Merits of this process contain mild reaction conditions, easy monitoring, and importantly low cost. Morphology, crystallographic structure, and the properties of final product acquired through hydrothermal route can be accomplished by altering the experimental limitations that involve the variance in time, reaction medium, temperature, and pressure, etc. Surfactants are familiarized with the arrangement to advance hydrothermal route. The surfactant-promoted method has been verified to results in an efficacious manner in order to fabricate metal oxide owing to an assortment of morphologies. Three phases are always involved in the system firstly, oil phase secondly, surfactant phase, and lastly, aqueous phase. In the progression of route, surfactants can restrain the growth of final product. Meanwhile, pH value, concentration of reactants, and temperature also has necessary guidance on the structure, properties, and morphology of the product [2, 67–69].

To prepare one dimensional (1-D) metal-oxide nanostructures such as wires/fibers [70, 71], nanorods [72–74], nanotubes [75, 76], hemitubes [77], nanobelts [78, 79], and needles/tips [70, 80], enormous attempts have been made. To enhance the morphological parameters, VS and VLS are the two main growth mechanisms used in vapor phase method. By changing variables such as assisting electric field, substrate, catalyst, pre-treatment, deposition temperature, etc., morphologies of required products can be controlled. Vapor phase method in the presence of oxygen obtained WO_3 1-D nanostructures which have high aspect ratios (**Figure 5a**) showed exceptional results in field emission display (**Figure 5b**) and also in some other applications such as gas sensors, photodetectors, and so on. It's convenient to comprehend monoclinic formation (three unequal axes) of γ-WO_3 phase which is stable at 17–320 °C by assuming the growth temperature under 1000 °C, transition of phase in WO_3 is not completely reversible while the most stable phase reported at room temperature is γ-WO_3 [2].

Heterogeneous substrates are used to grow 1-D nanostructures [70, 83], affected by the substrate surface, mostly, they exhibited {001} growth direction beside length (**Figure 5c**), while W + Si supported Au film or nanowires on Si wafer showed {010} or {100}/{010} growth direction (**Figure 5d, e**). Due to lack of oxygen gas WO_2 nanowires were synthesized caused by oxidation of Ni, by restoring the substrate with Si + W succeeded by Ni film (**Figure 5f**) [83]. By using vapor phase method, $WO_{3-\tau}$ ($0 < \tau < 1$) 1-D nanostructures (e.g. $W_{18}O_{29}$) can be manufactured with poor oxygen atmosphere (react with slighter oxygen source or gas like carbon dioxde) [84, 85]. Because of closely packed planes such as {010}, one-dimensional $W_{18}O_{29}$ nanostructures (e.g. nanoneedles, nanowire, nanotip, *etc.*, substrates

dependent) commonly revealed monoclinic (unequal axes) phase with the selective growth along {010} direction (**Figure 6**).

Substrates are conventionally utilized for growth of hierarchical structures in vapor phase method. On the Si substrate surface along with polystyrene spheres monolayer, 0-D and 2-D structures of α-Fe_2O_3 can be attained by PLD-CVD at an oxygen pressure 60 and 6 Pascal, respectively [87], as shown in **Figure 7a-d**. Since there is deficiency of Fe atoms and O atoms are in excess in {110} plane, so for preferential growth along {110} direction, it can be assumed to be driving force. Single dimensional-based 3-D Fe_3O_4 successfully synthesized in an autoclave on its wall (**Figure 7e** and **f**) through the pyrolysis of ferrocene (supercritical carbon dioxide at 450 °C) Cao *et al.* [88] increasing Fe sources resulted in the formation of 2-D nanosheets while decreasing the amount CO_2 sources led to the reduction of

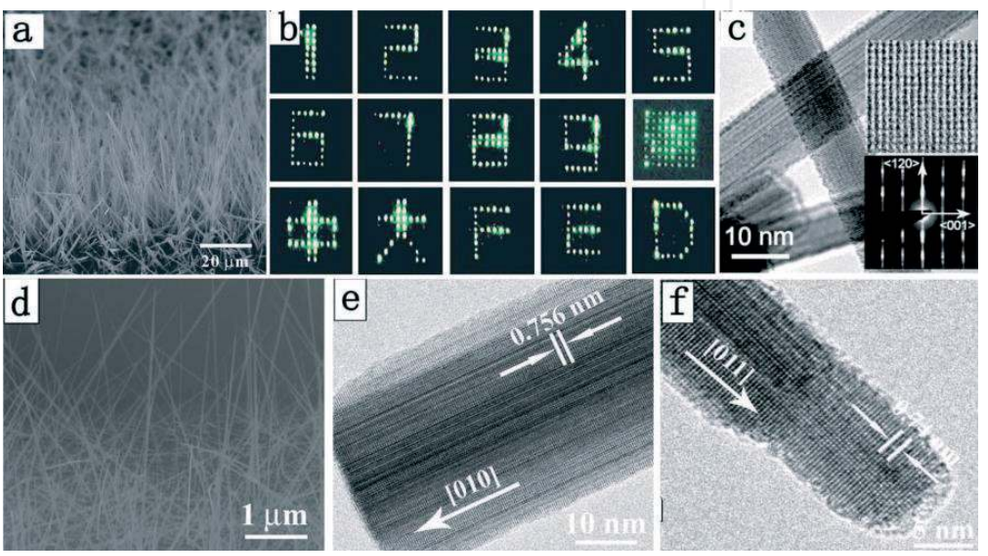

Figure 5.
(a) The cross-sectional SEM image of as-prepared WO_3 nanowires, and (b) Arabic numerals and Chinese characters displayed by the double-gated FED [81] (c) TEM micrographs showing the lattice fringes and the diffraction pattern (insets) of individual tungsten oxide nanowires [82] (d) the SEM image of γ-WO_3 nanowires, (e) typical HRTEM images of γ-WO_3 nanowire and (f) WO_2 nanowire [83].

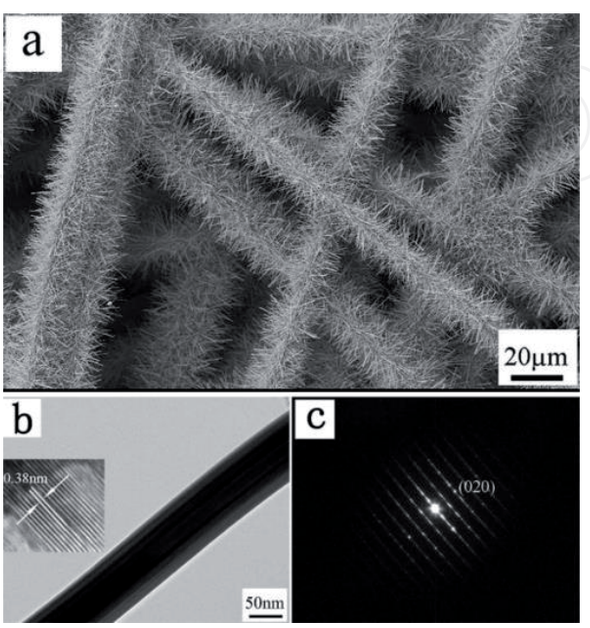

Figure 6.
(a) SEM images of three-dimensionally aligned $W_{18}O_{49}$ nanowires on carbon microfibers, (b) a typical TEM image of a single $W_{18}O_{49}$ nanowire (c) selected area electron diffraction (SAED) pattern of the nanowire [86].

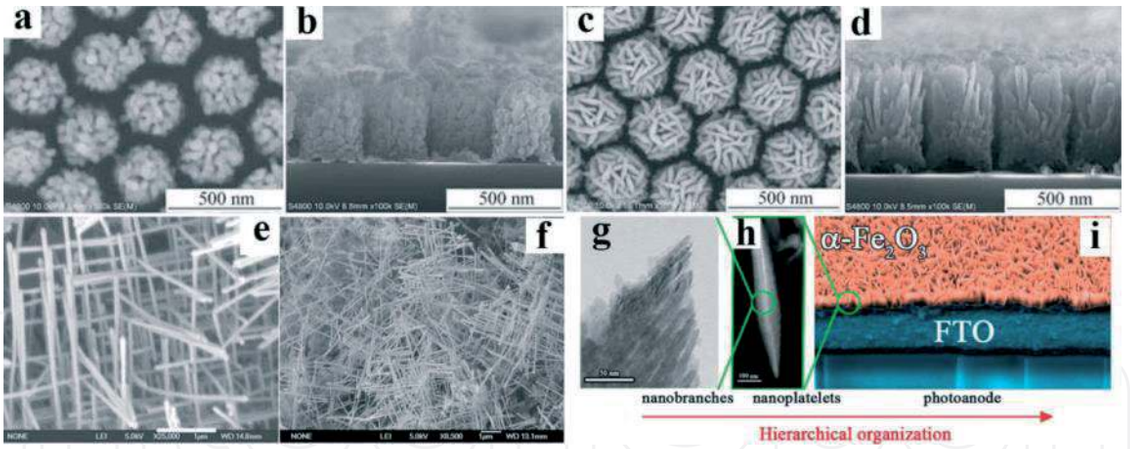

Figure 7.
(a) SEM images of as-deposited samples at an oxygen pressure of 6 Pa (0D based, a and b) and 60 Pa; (a), (c) top surface; (b), (d) cross-section [87]. (e and f) typical FESEM images of 3D Fe_3O_4 networks [88] (g) HRTEM image and (h) HAADF-STEM micrograph representing the hierarchical morphology of the hematite platelets; (i) a cross-sectional SEM image of hematite nanoplatelet arrays [89].

nanorods length. On the substrate of FTO (**Figure 7g–i**), nanoplatelet of α-Fe_2O_3 can be obtained at room temperature in a PECVD system, whose thickness can be increase by increasing the amount of Fe sources [89].

Multiple FeO_x arranged nanostructures can be prepared through simple solution method, precursor based method, template-directed, and solvo/hydrothermal reaction in liquid phase method. By precursor based method [90, 91] and solvo/hydrothermal reaction [92], 0-D based FeO_x arranged nanostructures (mesoporous particles such as spheres, cubes, super-structures, hollow spheres/bowls, etc. (**Figure 8a–c**) are commonly prepared. Metal–organic frameworks (MOFs) have received great attention as an advanced type of precursors with controllable properties such as shape, composition, size, and internal structure for MOX arranged nanostructures. For example, Fe_2O_3 microboxes synthesized by Lou *et al.* [95] with different shell structures (**Figure 8e–j**) based on appropriate annealing of pre-formed PB (Prussian blue) microcubes (**Figure 8d**) [2].

As-synthesized Fe_2O_3 micro boxes having unique shell structures and distinguish cycling performance unveiled high lithium storage capacities when evaluated for

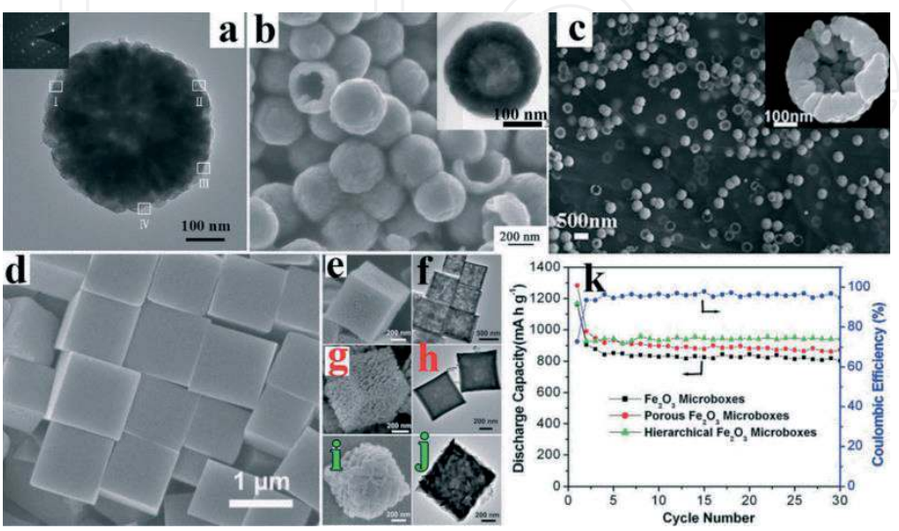

Figure 8.
(a) A TEM image of a single Fe_3O_4 microsphere, with a corresponding SAED pattern (inset) [91] (b) a SEM image of Fe_3O_4 hollow microspheres (the inset is the corresponding TEM image) [93] (c) SEM images of the bowl-like hollow Fe_3O_4/r-GO composites [94] (d) a FESEM images of PB microcubes; (e, g, i) FESEM and (f, h, j) TEM images of hollow Fe_2O_3 microboxes [95].

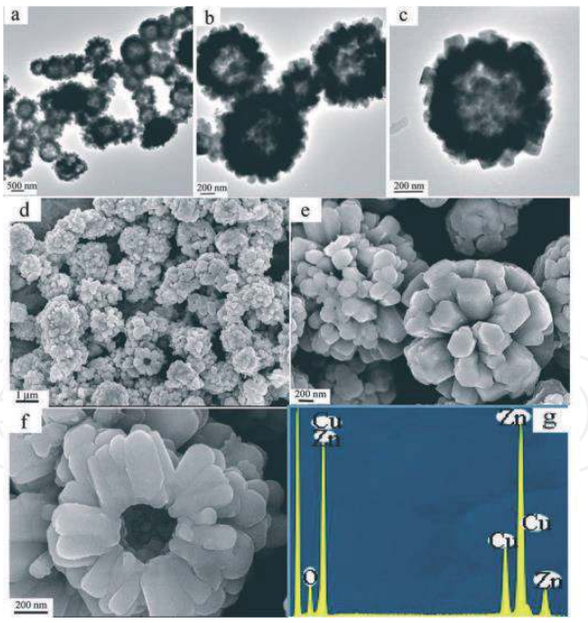

Figure 9.
Morphology of the hollow spheres composed of ZnO nanorods. (a) TEM image of the samples (b, c) typical magnified TEM images of hollow spheres (d, e) SEM image of the samples (f) typical magnified SEM image of a hollow sphere (g) the EDS spectrum of hollow spheres [98].

lithium-ion batteries as potential anode material. Furthermore, using controlled chemical etching, hollow interiors could be generated inside the PB nanoparticles in poly (vinylpyrrolidone) presence, [96] porous nanostructures of iron oxide having hollow interiors, various phases of these PB nanoparticles (preliminary precursors) can be synthesized by controlled calcination.

Due to the potential uses in various fields like waste removal, biologically active agent protection, chemical, biological sensors, catalysis, and bimolecular-release systems, well-defined 0-D ZnO hollow structures have attracted much attention. So in past few years, many successful attempts were made to prepare hollow structures of ZnO. The template-assisted technique is now the main focus of researchers which conventionally employed spherobacteria, carbon spheres, polystyrene spheres, and so on as template for hollow structures growth of ZnO. Under hydrothermal conditions, conversion of $Zn(NH_3)_4^{2+}$ reported by Gao *et al.* [97] resulted in hollow spheres of ZnO formation which have an inner and outer diameter as 100 nm and 600 nm, respectively. These hollow spheres were made up of ZnO nanorods (**Figure 9**). Ethanol volume ratio with respect to solution and initial mixture pH value both have a significant role in hollow spheres formation. Meanwhile, results obtained from characterization, ZnO hollow spheres showed remarkable photoluminescence properties (at room temperature) with UV emission peak at 390 nm.

4. Advanced applications

Over the past decade, due to unique electronic, magnetic, and optical applications metal oxide materials arising as potential candidates with fruitful functionalities have been extensively studied. These applications will be discussed briefly in this section.

4.1 Photovoltaics

In photovoltaics stable and environment-friendly metal oxide semiconductors are used in dye–sensitized solar cells (DSSCs) as photoelectrode or to design p-n

junctions of metal oxide. Materials have been examined for photoelectrodes purpose in DSSCs (**Figure 10**) such as binary metal oxides (ZrO_2, Fe_2O_3, TiO_2, Al_2O_3, ZnO, Nb_2O_5) and ternary compounds ($SrTiO_3$, Zn_2SnO_4). Due to high thermal and chemical stability, a hole blocking property, and suitable electron selectivity Nb_2O_5, ZnO, and TiO_2 are excellent expectant as a photoelectrode [2, 99, 100].

4.2 Lithium-ion batteries

In technology, lithium-ion batteries made up of metal oxide nanoparticles (SnO_2, Co_3O_4, Fe_2O_3, TiO_2, and complex metal oxides) enable superior rate capability; better cycling performance and high specific capacity are arising as the best choice for portable electronics. Its applications include electronics, electric vehicles, etc. Transition metal oxides hold boundless potential towards high-energy-density anode due to their better capacities than those which are commercially utilized as anode material such as graphite [2, 101, 102].

4.3 Photocatalysis

In most highlighted photocatalytic areas TiO_2 has been the most promising material as a photocatalyst. In last 3 decades, TiO_2 attracted notable scientific and technological consequences (**Figure 11**). Similarly, to study other photocatalytic oxidation properties metal oxides (ZnO, SnO_2, Fe_2O_3, WO_3, Cu_2O, $SrTiO_3$) have been studied in detail. High crystallinity and large surface area with more active sites reduce recombination rate of photo–generated electron–holes pairs are the properties of the best photocatalyst. For oxygen (O_2) evolution by photocatalysis from H_2O under irradiation of visible light, highly–arranged tungsten oxide (m – WO_3) hybridized with reduced graphene-oxide has been synthesized. Tremendous photocatalytic properties have been shown by CdS nanorods/reduced graphene-oxide composites had excellent photocatalytic properties with a rate constant was around three times greater than CdS nanorods for the degradation of MO [2, 103].

4.4 Gas-sensing

Electrical conductance sensitive to ambient gas composition, rising from interactions of charges with volatile organic compounds, reactive gases (O_2, CO, NO_x), hydrocarbons, and semiconducting metal oxides (WO_3, TiO_2, SnO_2, ZnO) are utilized for gas sensing applications. The effort was made to acquire better results towards low pollutant gas concentrations under low operating temperatures for gas sensing materials. For the detection of harmful gases and large scale, thermal stability under operating conditions of sensors SnO_2 nanostructures has attracted the most attention [2, 104].

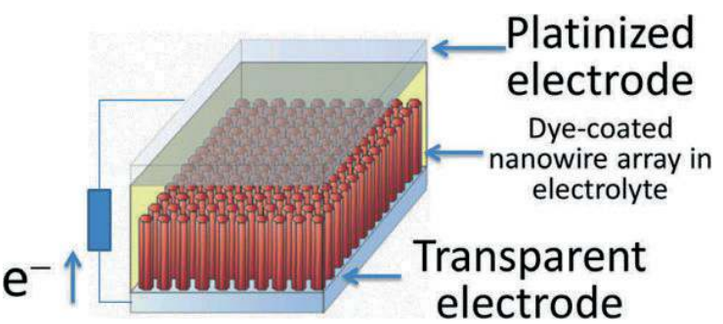

Figure 10.
Schematic diagram of the nanowire dye-sensitized solar cell based on a ZnO wire array [99].

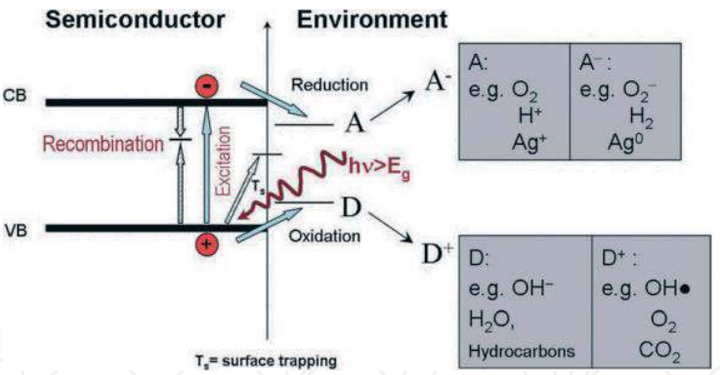

Figure 11.
Scheme of photo-induced processes at a TiO_2 semiconductor/electrolyte interface [103].

4.5 Biomedical

In biomedical field, magnetic metal oxides have been used with biological agents, have excellent applications. As superparamagnetic Fe_3O_4 can act as potent nanoprobes magnetic fluid hyperthermia (MFH), biosensors, magnetic resonance imaging (MRI) are biocompatible and stable chemically as well as magnetically. For therapy and targeted drug delivery, Ferrite MFe_2O_4 (where M = Mn, Zn, Ni, Co, etc.) has also been characterized and studied [105–107].

5. Outlook, challenges, and a little science fiction

The synergic effects and complex chemical configurations of several metal species in the TMOs induce noteworthy electrochemical performance. Numerous elegant approaches including compositions and manipulation of the micro/nano-structures have been widely established, that aims to endorse utilization of TMOs in everyday energy conversion technologies and enhancement of electrochemical performance. However, each designed approach applies lonely that normally consequences in partial enhancement in of electrodes based upon TMOs with respect to their electrochemical performance. Thus, it is more fascinating to assimilate manifold stimulating design approaches, therefore aggregating their electrochemical performance to meet today's energy demands.

The mainstream of research reports owing to the utilization of TMOs related to boost energy storage devices is primarily based on the observations of a specific experiment. A wide-ranging insight into the connection among the composition (structure) and properties of these TMOs that are related to their performance has not been systematically attained yet. Thus, effective and reliable methods and standards are necessary to develop urgently to assess the energy storage devices that are based on TMOs. Theoretical simulation and mathematical modeling are also greatly anticipated to be established in order to direct large-scale, low-cost, and facile fabrication along with the purposeful design of TMOs for greater electrochemical performance.

Realizing the unsuccessful mechanisms upon cycling in the electrodes based upon TMOs for LIBs is crucial to direct the scheme and design of progressive materials. This needs to understand the compositional parameter and structural evolution as well as consideration of electrolyte compatibility matter. The amendment of electrolytes including certain reversible redox-couples (as additives) in aqueous electrolytes has been demonstrated that could considerably progress the general electrochemical progress of pseudo-capacitive materials. Thus, we also assume that appropriate scheme and design of electrolytes could additionally elevate the electrochemical performance of TMOs for both rechargeable batteries. Additionally,

the assessment of pseudo-capacitive progress of TMOs is generally accomplished in aqueous electrolytes. This accomplishment is unescapably restricts the energy density owing to a slight stable potential window of aqueous electrolytes. Several other non-aqueous electrolytes that belong to organic class have been studied to boost output operating voltage which usually delivers 2–3 times broader working voltage window as compared to aqueous ones. Hence, the investigation of ECs that are based upon TMO (using organic electrolytes) is of great significance to attain greater energy density that will significantly cover the practical implementation of ECs. Besides the assessment based on electrochemical progress, other concerns about cost, and comfort, protection, and environmental compatibility of production and manipulation must also be engaged into thoughtful concern when TMOs are developing for LIBs to make them industrially applicable. It must be stressed about the synthesis mechanism of these TMO materials as it must be definitely scalable for commercial applications.

A complex method is the electrochemical reduction of oxygen over TMO catalysts that can comprise altered mechanisms that can be regulated through the nature of TMOs, owing to their adsorption and physicochemical properties. Till now, limited studies that are mainly attentive to the effect of catalyst features, mechanism, and kinetics of complex method discussed above. Further, adsorbed oxygen on the reaction rate, the intrinsic interactions between TMO catalysts and carbonaceous matrixes are also involved. The only trouble that is associated with examining the electrochemical procedures on TMOs are related to their semiconducting properties. These properties can lead to change in the behaviors of reactions on TMOs catalysts in comparison with the metal-based catalysts. Future progress might lead to extremely effective and inexpensive TMO catalysts after some heightened between the corrosion resistance, electro-catalytic experiment, fabrication cost, thermodynamic stability, and long-term stability.

Given the difficulties ahead, there is optimism that TMOs will be the materials forum soon for overcoming many of the existing bottlenecks problems in sustainable and renewable energy storage/conversion sectors. To accomplish this purpose, momentous improvements in electrochemical efficiency and a comprehensive understanding of TMOs dynamics in energy storage/conversion applications must be established. These fascinating TMO materials will provide a new path to make desirable energy innovations that will economically feasible with continued and committed research efforts.

Conflict of interest

Authors have declared no ‘conflict of interest.

Author details

Muhammad Ikram[1*], Ali Raza[2], Jahan Zeb Hassan[2], Arslan Ahmed Rafi[2], Asma Rafiq[1], Shehnila Altaf[3] and Atif Ashfaq[1]

1 Solar Cell Applications Research Lab, Department of Physics, Government College University Lahore, Lahore, Punjab, Pakistan

2 Department of Physics, Riphah Institute of Computing and Applied Sciences (RICAS), Riphah International University, Lahore, Pakistan

3 Department of Chemistry, University of Engineering and Technology, Lahore, Pakistan

*Address all correspondence to: dr.muhammadikram@gcu.edu.pk

References

[1] C. N. R. Rao, *Transition-metal oxides*. United States: Marcel Dekker, Inc, 1974.

[2] T. Guo, M.-S. Yao, Y.-H. Lin, and C.-W. Nan, "A comprehensive review on synthesis methods for transition-metal oxide nanostructures," *CrystEngComm,* 10.1039/C5CE00034C vol. 17, no. 19, pp. 3551-3585, 2015.

[3] P. A. Cox, *Transition metal oxides: an introduction to their electronic structure and properties*. Oxford university press, 2010.

[4] C. Yuan, H. B. Wu, Y. Xie, and X. W. Lou, "Mixed Transition-Metal Oxides: Design, Synthesis, and Energy-Related Applications," vol. 53, no. 6, pp. 1488-1504, 2014.

[5] E. Lee, Y. S. Yoon, and D.-J. Kim, "Two-Dimensional Transition Metal Dichalcogenides and Metal Oxide Hybrids for Gas Sensing," *ACS Sensors,* vol. 3, no. 10, pp. 2045-2060, 2018/10/26 2018.

[6] G. Korotcenkov, "Current Trends in Nanomaterials for Metal Oxide-Based Conductometric Gas Sensors: Advantages and Limitations. Part 1: 1D and 2D Nanostructures," *Nanomaterials (Basel),* vol. 10, no. 7, Jul 17 2020.

[7] N. Joshi, T. Hayasaka, Y. Liu, H. Liu, O. N. Oliveira, and L. Lin, "A review on chemiresistive room temperature gas sensors based on metal oxide nanostructures, graphene and 2D transition metal dichalcogenides," *Microchimica Acta,* vol. 185, no. 4, p. 213, 2018/03/10 2018.

[8] M. A. A. Mohd Abdah, N. H. N. Azman, S. Kulandaivalu, and Y. Sulaiman, "Review of the use of transition-metal-oxide and conducting polymer-based fibres for high-performance supercapacitors," *Materials & Design,* vol. 186, p. 108199, 2020/01/15/ 2020.

[9] S. Z. Hussain, M. Ihrar, S. B. Hussain, W. C. Oh, and K. Ullah, "A review on graphene based transition metal oxide composites and its application towards supercapacitor electrodes," *SN Applied Sciences,* vol. 2, no. 4, p. 764, 2020/03/27 2020.

[10] C. Goswami, K. K. Hazarika, and P. Bharali, "Transition metal oxide nanocatalysts for oxygen reduction reaction," *Materials Science for Energy Technologies,* vol. 1, no. 2, pp. 117-128, 2018/12/01/ 2018.

[11] W. Gao and Z. Li, "21 - Nano-structured transition metal oxides and their applications in composites," in *Physical Properties and Applications of Polymer Nanocomposites*, S. C. Tjong and Y. W. Mai, Eds.: Woodhead Publishing, 2010, pp. 723-742.

[12] M. Niederberger, "Metal Oxides: Chemistry and Applications. Edited by J. L. G. Fierro," vol. 8, no. 4, pp. 617-618, 2007.

[13] B. Xiao and X. Sun, "Surface and Subsurface Reactions of Lithium Transition Metal Oxide Cathode Materials: An Overview of the Fundamental Origins and Remedying Approaches," vol. 8, no. 29, p. 1802057, 2018.

[14] W. H. Low, P. S. Khiew, S. S. Lim, C. W. Siong, and E. R. Ezeigwe, "Recent development of mixed transition metal oxide and graphene/mixed transition metal oxide based hybrid nanostructures for advanced supercapacitors," *Journal of Alloys and Compounds,* vol. 775, pp. 1324-1356, 2019/02/15/ 2019.

[15] J. L. G. Fierro, *Metal oxides: chemistry and applications*. CRC press, 2005.

[16] M. A. Bañares and I. E. Wachs, "Molecular structures of supported metal oxide catalysts under different

environments," vol. 33, no. 5, pp. 359-380, 2002.

[17] A. Urban, A. Abdellahi, S. Dacek, N. Artrith, and G. Ceder, "Electronic-Structure Origin of Cation Disorder in Transition-Metal Oxides," *Physical Review Letters,* vol. 119, no. 17, p. 176402, 10/25/ 2017.

[18] J. P. Attfield, "Charge ordering in transition metal oxides," *Solid State Sciences,* vol. 8, no. 8, pp. 861-867, 2006/08/01/ 2006.

[19] T. Seike and J. Nagai, "Electro-chromism of 3d transition metal oxides," *Solar Energy Materials,* vol. 22, no. 2, pp. 107-117, 1991/07/01/ 1991.

[20] F. D. Hardcastle and I. E. J. T. J. o. P. C. Wachs, "Determination of vanadium-oxygen bond distances and bond orders by Raman spectroscopy," vol. 95, no. 13, pp. 5031-5041, 1991.

[21] Z. Jiang, "First-Principle Study of All-Vanadium Redox Flow Battery," The University of Nebraska-Lincoln, 2019.

[22] P. H. K. Charan and G. R. J. J. o. P. M. Rao, "Investigation of chromium oxide clusters grafted on SBA-15 using Cr-polycation sol," vol. 20, no. 1, pp. 81-94, 2013.

[23] N. M. Peek *et al.*, "Reassessment of the Electronic Structure of Cr(VI) Sites Supported on Amorphous Silica and Implications for Cr Coordination Number," *The Journal of Physical Chemistry C,* vol. 122, no. 8, pp. 4349-4358, 2018/03/01 2018.

[24] W. Lu, J. Li, Y. Sheng, X. Zhang, J. You, and L. Chen, "One-pot synthesis of magnetic iron oxide nanoparticle-multiwalled carbon nanotube composites for enhanced removal of Cr(VI) from aqueous solution," *Journal of Colloid and Interface Science,* vol. 505, pp. 1134-1146, 2017/11/01/ 2017.

[25] A. Chauhan *et al.*, "Microstructure characterization and strengthening mechanisms of oxide dispersion strengthened (ODS) Fe-9%Cr and Fe-14%Cr extruded bars," *Journal of Nuclear Materials,* vol. 495, pp. 6-19, 2017/11/01/ 2017.

[26] T. Varadavenkatesan, E. Lyubchik, S. Pai, A. Pugazhendhi, R. Vinayagam, and R. Selvaraj, "Photocatalytic degradation of Rhodamine B by zinc oxide nanoparticles synthesized using the leaf extract of Cyanometra ramiflora," *Journal of Photochemistry and Photobiology B: Biology,* vol. 199, p. 111621, 2019/10/01/ 2019.

[27] Y. Lin *et al.*, "Chromium-ruthenium oxide solid solution electrocatalyst for highly efficient oxygen evolution reaction in acidic media," *Nature Communications,* vol. 10, no. 1, p. 162, 2019/01/11 2019.

[28] M. Rimoldi, J. T. Hupp, and O. K. Farha, "Atomic Layer Deposition of Rhenium–Aluminum Oxide Thin Films and ReOx Incorporation in a Metal–Organic Framework," *ACS Applied Materials & Interfaces,* vol. 9, no. 40, pp. 35067-35074, 2017/10/11 2017.

[29] Y. Gao *et al.*, "Interaction Mechanism of Re(VII) with Zirconium Dioxide Nanoparticles Archored onto Reduced Graphene Oxides," *ACS Sustainable Chemistry & Engineering,* vol. 5, no. 3, pp. 2163-2171, 2017/03/06 2017.

[30] D. Schildhammer, G. Fuhrmann, L. Petschnig, N. Weinberger, H. Schottenberger, and H. Huppertz, "Synthesis and characterization of a new high NIR reflective ytterbium molybdenum oxide and related doped pigments," *Dyes and Pigments,* vol. 138, pp. 90-99, 2017/03/01/ 2017.

[31] K. Inzani, M. Nematollahi, F. Vullum-Bruer, T. Grande, T. W. Reenaas, and S. M. Selbach, "Electronic properties of reduced molybdenum

oxides," *Physical Chemistry Chemical Physics,* 10.1039/C7CP00644F vol. 19, no. 13, pp. 9232-9245, 2017.

[32] Y. Li *et al.*, "Manipulation of Surface Plasmon Resonance in Sub-Stoichiometry Molybdenum Oxide Nanodots through Charge Carrier Control Technique," *The Journal of Physical Chemistry C,* vol. 121, no. 9, pp. 5208-5214, 2017/03/09 2017.

[33] D. S. Kim, T. C. Ozawa, K. Fukuda, S. Ohshima, I. Nakai, and T. Sasaki, "Soft-Chemical Exfoliation of Na0.9Mo2O4: Preparation and Electrical Conductivity Characterization of a Molybdenum Oxide Nanosheet," *Chemistry of Materials,* vol. 23, no. 11, pp. 2700-2702, 2011/06/14 2011.

[34] S. J. Xiao, X. J. Zhao, P. P. Hu, Z. J. Chu, C. Z. Huang, and L. Zhang, "Highly Photoluminescent Molybdenum Oxide Quantum Dots: One-Pot Synthesis and Application in 2,4,6-Trinitrotoluene Determination," *ACS Applied Materials & Interfaces,* vol. 8, no. 12, pp. 8184-8191, 2016/03/30 2016.

[35] E. Yavuz, K. V. Özdokur, İ. Çakar, S. Koçak, and F. N. Ertaş, "Electrochemical Preparation, Characterization of Molybdenum-Oxide/Platinum Binary Catalysts and Its Application to Oxygen Reduction Reaction in Weakly Acidic Medium," *Electrochimica Acta,* vol. 151, pp. 72-80, 2015/01/01/ 2015.

[36] E. Rossinyol *et al.*, "Synthesis and Characterization of Chromium-Doped Mesoporous Tungsten Oxide for Gas Sensing Applications," vol. 17, no. 11, pp. 1801-1806, 2007.

[37] S. H. Baeck, T. F. Jaramillo, C. Brändli, and E. W. McFarland, "Combinatorial Electrochemical Synthesis and Characterization of Tungsten-Based Mixed-Metal Oxides," *Journal of Combinatorial Chemistry,* vol. 4, no. 6, pp. 563-568, 2002/11/01 2002.

[38] A. Baserga *et al.*, "Nanostructured tungsten oxide with controlled properties: Synthesis and Raman characterization," *Thin Solid Films,* vol. 515, no. 16, pp. 6465-6469, 2007/06/04/ 2007.

[39] H. M. A. Soliman, A. B. Kashyout, M. S. El Nouby, and A. M. Abosehly, "Preparation and characterizations of tungsten oxide electrochromic nanomaterials," *Journal of Materials Science: Materials in Electronics,* vol. 21, no. 12, pp. 1313-1321, 2010/12/01 2010.

[40] F. Di Fonzo *et al.*, "Synthesis and characterization of tungsten and tungsten oxide nanostructured films," *Catalysis Today,* vol. 116, no. 1, pp. 69-73, 2006/07/30/ 2006.

[41] M. N. Kozicki, C. Gopalan, M. Balakrishnan, and M. Mitkova, "A Low-Power Nonvolatile Switching Element Based on Copper-Tungsten Oxide Solid Electrolyte," *IEEE Transactions on Nanotechnology,* vol. 5, no. 5, pp. 535-544, 2006.

[42] C. Gao, Q. Han, and M. Wu, "Review on transition metal compounds based counter electrode for dye-sensitized solar cells," *Journal of Energy Chemistry,* vol. 27, no. 3, pp. 703-712, 2018/05/01/ 2018.

[43] C. N. R. Rao, "Transition Metal Oxides," vol. 40, no. 1, pp. 291-326, 1989.

[44] L. Qiao and M. T. Swihart, "Solution-phase synthesis of transition metal oxide nanocrystals: Morphologies, formulae, and mechanisms," *Advances in Colloid and Interface Science,* vol. 244, pp. 199-266, 2017/06/01/ 2017.

[45] C. N. R. Rao, "Transition Metal Oxides," *Annual Review of Physical Chemistry,* vol. 40, no. 1, pp. 291-326, 1989/10/01 1989.

[46] M. S. Whittingham, "Hydrothermal synthesis of transition metal oxides under mild conditions," *Current Opinion*

in Solid State and Materials Science, vol. 1, no. 2, pp. 227-232, 1996/04/01/ 1996.

[47] A. Zavabeti *et al.*, "A liquid metal reaction environment for the room-temperature synthesis of atomically thin metal oxides," *Science,* vol. 358, no. 6361, p. 332, 2017.

[48] J. H. Zheng, R. M. Zhang, P. F. Yu, and X. G. Wang, "Binary transition metal oxides (BTMO) (Co-Zn, Co-Cu) synthesis and high supercapacitor performance," *Journal of Alloys and Compounds,* vol. 772, pp. 359-365, 2019/01/25/ 2019.

[49] T. Kida, T. Doi, and K. Shimanoe, "Synthesis of monodispersed SnO2 nanocrystals and their remarkably high sensitivity to volatile organic compounds," *Chemistry of Materials,* vol. 22, no. 8, pp. 2662-2667, 2010/04/27 2010.

[50] T. R. Gordon *et al.*, "Nonaqueous Synthesis of TiO2 Nanocrystals Using TiF4 to Engineer Morphology, Oxygen Vacancy Concentration, and Photocatalytic Activity," *Journal of the American Chemical Society,* vol. 134, no. 15, pp. 6751-6761, 2012/04/18 2012.

[51] G. Mavrou *et al.*, "Electrical properties of La2O3 and HfO2/La2O3 gate dielectrics for germanium metal-oxide-semiconductor devices," vol. 103, no. 1, p. 014506, 2008.

[52] J. S. Yeoh, C. F. Armer, and A. Lowe, "Transition metal oxalates as energy storage materials. A review," *Materials Today Energy,* vol. 9, pp. 198-222, 2018/09/01/ 2018.

[53] M.-J. Lee *et al.*, "Electrical Manipulation of Nanofilaments in Transition-Metal Oxides for Resistance-Based Memory," *Nano Letters,* vol. 9, no. 4, pp. 1476-1481, 2009/04/08 2009.

[54] M. Gutowski *et al.*, "Thermodynamic stability of high-K dielectric metal oxides ZrO2 and HfO2 in contact with Si and SiO2," vol. 80, no. 11, pp. 1897-1899, 2002.

[55] D. Zappa, V. Galstyan, N. Kaur, H. M. M. Munasinghe Arachchige, O. Sisman, and E. Comini, ""Metal oxide -based heterostructures for gas sensors"- A review," *Analytica Chimica Acta,* vol. 1039, pp. 1-23, 2018/12/18/ 2018.

[56] V. V. Sysoev, B. K. Button, K. Wepsiec, S. Dmitriev, and A. Kolmakov, "Toward the Nanoscopic "Electronic Nose": Hydrogen vs Carbon Monoxide Discrimination with an Array of Individual Metal Oxide Nano- and Mesowire Sensors," *Nano Letters,* vol. 6, no. 8, pp. 1584-1588, 2006/08/01 2006.

[57] R. Paulose, R. Mohan, and V. Parihar, "Nanostructured nickel oxide and its electrochemical behaviour—A brief review," *Nano-Structures & Nano-Objects,* vol. 11, pp. 102-111, 2017/07/01/ 2017.

[58] A. V. Emeline, G. V. Kataeva, A. V. Panasuk, V. K. Ryabchuk, N. V. Sheremetyeva, and N. Serpone, "Effect of Surface Photoreactions on the Photocoloration of a Wide Band Gap Metal Oxide: Probing Whether Surface Reactions Are Photocatalytic," *The Journal of Physical Chemistry B,* vol. 109, no. 11, pp. 5175-5185, 2005/03/01 2005.

[59] M. Kröger, S. Hamwi, J. Meyer, T. Riedl, W. Kowalsky, and A. Kahn, "P-type doping of organic wide band gap materials by transition metal oxides: A case-study on Molybdenum trioxide," *Organic Electronics,* vol. 10, no. 5, pp. 932-938, 2009/08/01/ 2009.

[60] L. Dai, X. L. Chen, J. K. Jian, M. He, T. Zhou, and B. Q. Hu, "Fabrication and characterization of In2O3 nanowires," *Applied Physics A,* vol. 75, no. 6, pp. 687-689, 2002/12/01 2002.

[61] X. Liu, C. Li, S. Han, J. Han, and C. Zhou, "Synthesis and electronic transport studies of CdO nanoneedles," vol. 82, no. 12, pp. 1950-1952, 2003.

[62] J.-M. Wu, H. C. Shih, W.-T. Wu, Y.-K. Tseng, and I. C. Chen, "Thermal evaporation growth and the luminescence property of TiO2 nanowires," *Journal of Crystal Growth,* vol. 281, no. 2, pp. 384-390, 2005/08/01/ 2005.

[63] S. Y. Bae, H. W. Seo, and J. Park, "Vertically Aligned Sulfur-Doped ZnO Nanowires Synthesized via Chemical Vapor Deposition," *The Journal of Physical Chemistry B,* vol. 108, no. 17, pp. 5206-5210, 2004/04/01 2004.

[64] Z. R. Dai, J. L. Gole, J. D. Stout, and Z. L. Wang, "Tin Oxide Nanowires, Nanoribbons, and Nanotubes," *The Journal of Physical Chemistry B,* vol. 106, no. 6, pp. 1274-1279, 2002/02/01 2002.

[65] A. Umar, S. H. Kim, Y. S. Lee, K. S. Nahm, and Y. B. Hahn, "Catalyst-free large-quantity synthesis of ZnO nanorods by a vapor–solid growth mechanism: Structural and optical properties," *Journal of Crystal Growth,* vol. 282, no. 1, pp. 131-136, 2005/08/15/ 2005.

[66] H. Ji, W. Zeng, and Y. Li, "Gas sensing mechanisms of metal oxide semiconductors: a focus review," *Nanoscale,* 10.1039/C9NR07699A vol. 11, no. 47, pp. 22664-22684, 2019.

[67] G. Zhang, X. Xiao, B. Li, P. Gu, H. Xue, and H. Pang, "Transition metal oxides with one-dimensional/one-dimensional-analogue nanostructures for advanced supercapacitors," *Journal of Materials Chemistry A,* 10.1039/C7TA02454A vol. 5, no. 18, pp. 8155-8186, 2017.

[68] M. Zheng *et al.*, "Hierarchically Nanostructured Transition Metal Oxides for Lithium-Ion Batteries," vol. 5, no. 3, p. 1700592, 2018.

[69] Z. Sun, T. Liao, and L. Kou, "Strategies for designing metal oxide nanostructures," *Science China Materials,* vol. 60, no. 1, pp. 1-24, 2017/01/01 2017.

[70] T. Stoycheva *et al.*, "Micromachined gas sensors based on tungsten oxide nanoneedles directly integrated via aerosol assisted CVD," *Sensors and Actuators B: Chemical,* vol. 198, pp. 210-218, 2014/07/31/ 2014.

[71] K. Zhu *et al.*, "Crystalline WO3 nanowires synthesized by templating method," *Chemical Physics Letters,* vol. 377, no. 3, pp. 317-321, 2003/08/15/ 2003.

[72] K. Huang, Q. Pan, F. Yang, S. Ni, X. Wei, and D. He, "Controllable synthesis of hexagonal WO3nanostructures and their application in lithium batteries," *Journal of Physics D: Applied Physics,* vol. 41, no. 15, p. 155417, 2008/07/17 2008.

[73] F. Zheng, H. Lu, M. Guo, and M. Zhang, "Effect of substrate pre-treatment on controllable synthesis of hexagonal WO3 nanorod arrays and their electrochromic properties," *CrystEngComm,* 10.1039/C3CE40494C vol. 15, no. 29, pp. 5828-5837, 2013.

[74] S. Rajagopal, D. Nataraj, D. Mangalaraj, Y. Djaoued, J. Robichaud, and O. Y. Khyzhun, "Controlled Growth of WO3Nanostructures with Three Different Morphologies and Their Structural, Optical, and Photodecomposition Studies," *Nanoscale Research Letters,* vol. 4, no. 11, p. 1335, 2009/08/04 2009.

[75] J. Li, X. Liu, Q. Han, X. Yao, and X. Wang, "Formation of WO3 nanotube-based bundles directed by NaHSO4 and its application in water treatment," *Journal of Materials Chemistry A,* 10.1039/C2TA00382A vol. 1, no. 4, pp. 1246-1253, 2013.

[76] Z.-G. Zhao and M. Miyauchi, "Nanoporous-Walled Tungsten Oxide Nanotubes as Highly Active Visible-Light-Driven Photocatalysts," *Angewandte Chemie International Edition,* https://doi.org/10.1002/anie.200802207 vol. 47, no. 37, pp. 7051-7055, 2008/09/01 2008.

[77] S.-J. Choi *et al.*, "Selective Diagnosis of Diabetes Using Pt-Functionalized WO3 Hemitube Networks As a Sensing Layer of Acetone in Exhaled Breath," *Analytical Chemistry,* vol. 85, no. 3, pp. 1792-1796, 2013/02/05 2013.

[78] J. Su, X. Feng, J. D. Sloppy, L. Guo, and C. A. Grimes, "Vertically Aligned WO3 Nanowire Arrays Grown Directly on Transparent Conducting Oxide Coated Glass: Synthesis and Photoelectrochemical Properties," *Nano Letters,* vol. 11, no. 1, pp. 203-208, 2011/01/12 2011.

[79] Y. B. Li, Y. Bando, D. Golberg, and K. Kurashima, "WO3 nanorods/nanobelts synthesized via physical vapor deposition process," *Chemical Physics Letters,* vol. 367, no. 1, pp. 214-218, 2003/01/02/ 2003.

[80] A. J. T. Naik, M. E. A. Warwick, S. J. A. Moniz, C. S. Blackman, I. P. Parkin, and R. Binions, "Nanostructured tungsten oxide gas sensors prepared by electric field assisted aerosol assisted chemical vapour deposition," *Journal of Materials Chemistry A,* 10.1039/C2TA01126C vol. 1, no. 5, pp. 1827-1833, 2013.

[81] J. Chen *et al.*, "Field emission display device structure based on double-gate driving principle for achieving high brightness using a variety of field emission nanoemitters," vol. 90, no. 25, p. 253105, 2007.

[82] C. Klinke, J. B. Hannon, L. Gignac, K. Reuter, and P. Avouris, "Tungsten Oxide Nanowire Growth by Chemically Induced Strain," *The Journal of Physical Chemistry B,* vol. 109, no. 38, pp. 17787-17790, 2005/09/01 2005.

[83] F. Liu, L. Li, F. Mo, J. Chen, S. Deng, and N. Xu, "A Catalyzed-Growth Route to Directly Form Micropatterned WO2 and WO3 Nanowire Arrays with Excellent Field Emission Behaviors at Low Temperature," *Crystal Growth & Design,* vol. 10, no. 12, pp. 5193-5199, 2010/12/01 2010.

[84] G. Gu, B. Zheng, W. Q. Han, S. Roth, and J. Liu, "Tungsten Oxide Nanowires on Tungsten Substrates," *Nano Letters,* vol. 2, no. 8, pp. 849-851, 2002/08/01 2002.

[85] X. Zhang *et al.*, "Tungsten Oxide Nanowires Grown on Carbon Cloth as a Flexible Cold Cathode," vol. 22, no. 46, pp. 5292-5296, 2010.

[86] Y. Zhang *et al.*, "Three-Dimensional Hierarchical Structure of Single Crystalline Tungsten Oxide Nanowires: Construction, Phase Transition, and Voltammetric Behavior," *The Journal of Physical Chemistry C,* vol. 113, no. 5, pp. 1746-1750, 2009/02/05 2009.

[87] L. Li and N. Koshizaki, "Vertically aligned and ordered hematite hierarchical columnar arrays for applications in field-emission, superhydrophilicity, and photocatalysis," *Journal of Materials Chemistry,* 10.1039/B922322C vol. 20, no. 15, pp. 2972-2978, 2010.

[88] F. Cao, Y. Liu, W. Hu, and Q. Chen, "Morphogenesis of Branched Coaxial Nanorods Formed in Supercritical Carbon Dioxide," *The Journal of Physical Chemistry C,* vol. 112, no. 7, pp. 2337-2342, 2008/02/01 2008.

[89] M. Marelli *et al.*, "Hierarchical Hematite Nanoplatelets for Photoelectrochemical Water Splitting," *ACS Applied Materials & Interfaces,* vol. 6, no. 15, pp. 11997-12004, 2014/08/13 2014.

[90] M. Hu, A. A. Belik, M. Imura, K. Mibu, Y. Tsujimoto, and Y. Yamauchi, "Synthesis of Superparamagnetic Nanoporous Iron Oxide Particles with Hollow Interiors by Using Prussian Blue Coordination Polymers," *Chemistry of Materials,* vol. 24, no. 14, pp. 2698-2707, 2012/07/24 2012.

[91] Q. Q. Xiong *et al.*, "Synthesis of Hierarchical Hollow-Structured Single-Crystalline Magnetite (Fe3O4) Microspheres: The Highly Powerful Storage versus Lithium as an Anode for Lithium Ion Batteries," *The Journal of*

Physical Chemistry C, vol. 116, no. 10, pp. 6495-6502, 2012/03/15 2012.

[92] Y. Liu *et al.*, "Synthesis of High Saturation Magnetization Superparamagnetic Fe3O4 Hollow Microspheres for Swift Chromium Removal," *ACS Applied Materials & Interfaces,* vol. 4, no. 9, pp. 4913-4920, 2012/09/26 2012.

[93] P. Hu, L. Yu, A. Zuo, C. Guo, and F. Yuan, "Fabrication of Monodisperse Magnetite Hollow Spheres," *The Journal of Physical Chemistry C,* vol. 113, no. 3, pp. 900-906, 2009/01/22 2009.

[94] H.-L. Xu, H. Bi, and R.-B. Yang, "Enhanced microwave absorption property of bowl-like Fe3O4 hollow spheres/reduced graphene oxide composites," vol. 111, no. 7, p. 07A522, 2012.

[95] L. Zhang, H. B. Wu, S. Madhavi, H. H. Hng, and X. W. Lou, "Formation of Fe2O3 Microboxes with Hierarchical Shell Structures from Metal–Organic Frameworks and Their Lithium Storage Properties," *Journal of the American Chemical Society,* vol. 134, no. 42, pp. 17388-17391, 2012/10/24 2012.

[96] M. Hu *et al.*, "Synthesis of Prussian Blue Nanoparticles with a Hollow Interior by Controlled Chemical Etching," vol. 51, no. 4, pp. 984-988, 2012.

[97] Y. Yin *et al.*, "Controlled synthesis and photoluminescence properties of BaXO4 (X=W, Mo) hierarchical nanostructures via a facile solution route," *Materials Letters,* vol. 64, no. 6, pp. 789-792, 2010/03/31/ 2010.

[98] Z. Chen and L. Gao, "A New Route toward ZnO Hollow Spheres by a Base-Erosion Mechanism," *Crystal Growth & Design,* vol. 8, no. 2, pp. 460-464, 2008/02/01 2008.

[99] M. Law, L. E. Greene, J. C. Johnson, R. Saykally, and P. Yang, "Nanowire dye-sensitized solar cells," *Nature Materials,* vol. 4, no. 6, pp. 455-459, 2005/06/01 2005.

[100] T. Gershon, "Metal oxide applications in organic-based photovoltaics," *Materials Science and Technology,* vol. 27, no. 9, pp. 1357-1371, 2011/09/01 2011.

[101] Y. Zhao *et al.*, "Recent Developments and Understanding of Novel Mixed Transition-Metal Oxides as Anodes in Lithium Ion Batteries," vol. 6, no. 8, p. 1502175, 2016.

[102] P. Poizot, S. Laruelle, S. Grugeon, L. Dupont, and J. M. Tarascon, "Nano-sized transition-metal oxides as negative-electrode materials for lithium-ion batteries," *Nature,* vol. 407, no. 6803, pp. 496-499, 2000/09/01 2000.

[103] I. Paramasivam, H. Jha, N. Liu, and P. Schmuki, "A Review of Photocatalysis using Self-organized TiO2 Nanotubes and Other Ordered Oxide Nanostructures," vol. 8, no. 20, pp. 3073-3103, 2012.

[104] E. Rossinyol *et al.*, "Nanostructured metal oxides synthesized by hard template method for gas sensing applications," *Sensors and Actuators B: Chemical,* vol. 109, no. 1, pp. 57-63, 2005/08/24/ 2005.

[105] K. Kannan, D. Radhika, K. K. Sadasivuni, K. R. Reddy, and A. V. Raghu, "Nanostructured metal oxides and its hybrids for photocatalytic and biomedical applications," *Advances in Colloid and Interface Science,* vol. 281, p. 102178, 2020/07/01/ 2020.

[106] S. Keskin and S. Kızılel, "Biomedical Applications of Metal Organic Frameworks," *Industrial & Engineering Chemistry Research,* vol. 50, no. 4, pp. 1799-1812, 2011/02/16 2011.

[107] S. Andreescu, M. Ornatska, J. S. Erlichman, A. Estevez, and J. C. Leiter, "Biomedical Applications of Metal Oxide Nanoparticles," in *Fine Particles in Medicine and Pharmacy*, E. Matijević, Ed. Boston, MA: Springer US, 2012, pp. 57-100.